International Journal of Nanomedicine

Dovepress
open access to scientific and medical research

Open Access Full Text Article

ORIGINAL RESEARCH

Numerical optimization of targeted delivery of charged nanoparticles to the ostiomeatal complex for treatment of rhinosinusitis

International Journal of Nanomedicine downloaded from https://www.dovepress.com/
For personal use only.

This article was published in the following Dove Press journal:
International Journal of Nanomedicine
30 July 2015
Number of times this article has been viewed

Jinxiang Xi[1]
Jiayao Eddie Yuan[1]
Xiuhua April Si[2]
James Hasbany[1]

[1]School of Engineering and Technology, Central Michigan University, Mount Pleasant, MI, [2]Department of Mechanical Engineering, California Baptist University, Riverside, CA, USA

Background: Despite the prevalence of rhinosinusitis that affects 10%–15% of the population, current inhalation therapy shows limited efficacy. Standard devices deliver <5% of the drugs to the sinuses due to the complexity of nose structure, secluded location of the sinus, poor ventilation, and lack of control of particle motions inside the nasal cavity.

Methods: An electric-guided delivery system was developed to guide charged particles to the ostiomeatal complex (OMC). Its performance was numerically assessed in an MRI-based nose–sinus model. Key design variables related to the delivery device, drug particles, and patient breathing were determined using sensitivity analysis. A two-stage optimization of design variables was conducted to obtain the best performance of the delivery system using the Nelder-Mead algorithm.

Results and discussion: The OMC delivery system exhibited high sensitivity to the applied electric field and electrostatic charges carried by the particles. Through the synthesis of electric guidance and point drug release, the new delivery system eliminated particle deposition in the nasal valve and turbinate regions and significantly enhanced the OMC doses. An OMC delivery efficiency of 72.4% was obtained with the optimized design, which is one order of magnitude higher than the standard nasal devices. Moreover, optimization is imperative to achieve a sound delivery protocol because of the large number of design variables. The OMC dose increased from 45.0% in the baseline model to 72.4% in the optimized system. The optimization framework developed in this study can be easily adapted for the delivery of drugs to other sites in the nose such as the ethmoid sinus and olfactory region.

Keywords: maxillary sinus, rhinosinusitis, intranasal aerosol drug delivery, charged particles, electric guidance, ostiomeatal complex

Introduction

Rhinosinusitis is a common respiratory disease in upper airways and affects 10%–15% of the population worldwide. Around 30 million people in the US suffer from chronic sinusitis, which leads to 0.6 million sinus surgeries and incurs $5.8 billion in health-care costs per year.[1] Women are nearly twice as likely as men to have rhinosinusitis.[2] Patients with rhinosinusitis will experience swollen mucosa, excessive mucus secretion, obstructed airway, and blocked drainage from sinus. Symptoms include stuffy nose, coughing, headache, lost sense of smell, facial swelling, sore throat, halitosis, constant tiredness, and fever.[3] On some occasions, acute sinusitis can lead to brain infection and other serious complications.[4] Among all paranasal sinuses, the maxillary sinus has the largest volume and is more prone to lesions than other sinuses from anatomical obstruction, bacterial or fungal colonization, viral infection, and exposure to allergens and irritants. Moreover, the maxillary sinus does not drain well due to

Correspondence: Jinxiang Xi
School of Engineering and Technology, Central Michigan University, 1200 South Franklin Street, Mount Pleasant, MI 48858, USA
Tel +1 989 774 2456
Fax +1 989 774 4900
Email xi1j@cmich.edu

© 2015 Xi et al. This work is published by Dove Medical Press Limited, and licensed under Creative Commons Attribution – Non Commercial (unported, v3.0) License. The full terms of the License are available at http://creativecommons.org/licenses/by-nc/3.0/. Non-commercial uses of the work are permitted without any further permission from Dove Medical Press Limited, provided the work is properly attributed. Permissions beyond the scope of the License are administered by Dove Medical Press Limited. Information on how to request permission may be found at: http://www.dovepress.com/permissions.php

the high location of the ostium. Due to the proximity to the maxillary teeth as well as frontal and ethmoidal sinuses, infections in the maxillary sinus can easily spread to these neighbors. Although paranasal sinus cancers are rare, they are most commonly found in the maxillary sinuses.[5]

Treatment of rhinosinusitis includes recovering sinus drainage, eliminating inflammation sources, decongesting the airway, and relieving the pain, which can be achieved by aerosolized inhalation therapy, surgery intervention, saline irrigation, or oral therapy. Inhalation therapy has multiple advantages over oral therapy, such as faster action onset, targeted drug delivery to the inflamed tissue, and lower systemic side effects. However, inhalation treatments with topical medications show only modest therapeutic efficacy, and there is a high rate of functional sinus surgeries in patients with rhinosinusitis. Because the middle meatus (MM) and sinus are poorly ventilated during normal breathing, drug delivery to these regions is limited. Most nasally administered drugs, like nasal sprays, are filtered by the nasal valve and cannot reach the MM or sinuses.[1] Nebulizers with small particles and swirling flows have demonstrated significantly improved aerosol delivery beyond the nasal valve region. They also delivered perceivable doses to the sinus; however, the sinus dose is very low (<1%). Moreover, there are considerable unintended depositions into the lungs, which can lead to the irritation of lung tissues. Concerns of pulmonary function deterioration have been raised related to extended inhalation of steroids and insulin.[6] One approach to avoid lung deposition is the bidirectional nasal delivery technique, where drugs are released only during oral exhalation with the soft palate closing the nose from the lower airway.[7] The setback of this approach is that >95% of the drugs will deposit in regions other than the target site, causing significant waste and adverse side effects.[8] More recently, sinus delivery with humming flow or pulsating aerosols is under active investigations, which have demonstrated improved delivery efficiencies to the paranasal sinuses.[3,9–12] However, even with these novel strategies, the delivery efficiency to the MM and sinus is limited, that is, <5%, aside from the substantial drug wastes in other regions of the respiratory tract and the associated adverse side effects.[1]

Among all the complexities of the nose anatomy, there are three challenges that are considered to preclude effective delivery of drugs to the maxillary sinus: the nasal valve, the slit-like opening to the MM, and the narrow ostium to the sinus. The nasal valve has the minimum cross-section area in the nasal chamber and behaves as the flow-limiting sector of the nose. The vena-contracta effects associated with the nasal valve induce elevated particle deposition in the nasal valve area due to the enhanced particle inertial impaction. Previous clinical studies showed that a majority of administered medications with metered-dose inhalers and nasal sprays were wasted in the nasal vestibule and valve regions.[1] The second challenge is the slit-opening to the MM, which is formed by two overlapping flaps of turbinate tissues (middle and inferior conchae) and prevents effective air ventilation and particle transport to the MM. During natural breathing, the majority of the air passes through the nasal median passage and only a small fraction of air is ventilated into the MM via the slit opening. The third challenge is the thin ostium to the sinus. Mucus and air from the maxillary sinuses drain into the nose under the middle turbinate through the ostium, which is located high on the nasal lateral wall and opens to the *hiatus semilunaris* of the MM. The maxillary sinus ostium is a funnel-shaped passage about 3–6 mm in diameter and 1–22 mm in length.[13] The area under the middle turbinate is the ostiomeatal complex (OMC), as shown in Figure 1A. Mucus blockage and bacteria proliferation in the OMC are frequent causes of infection in the maxillary sinus. Furthermore, the OMC itself is the most common area for sinusitis disorders and is the primary target for aerosolized drug therapy.[13]

Electric control of charged particles has been suggested for the targeted drug delivery to the human nose and lungs.[14–16] Enhanced particle depositions in the airways due to electrostatic charges were demonstrated in animals and humans, in vitro replicas of airways, and numerical modeling.[17–27] Realizing that poor olfactory doses are primarily due to the absence of control of particle motions after their release, Xi et al numerically studied the electrophoretic guidance of charged particles by applying an electric field to the nose.[28] In combination with focal drug release, it was demonstrated that the olfactory dosage could reach 90% efficiency. In the same manner, guidance of ferromagnetic drug particles with an appropriate magnetic field could also have the potential to target particles to the olfactory mucosa. The magnetic force required to do so can be achieved by carefully pairing the magnet strength with particle properties.[29] Recently, Xi et al numerically demonstrated that it is practical to improve the olfactory delivery efficiency to 45% with magnetophoretic guidance.[30] With optimized designs, the delivery efficiency to the olfactory region can be further improved to 67%.[31] Considering the secluded positions of the OMC and sinus, as well as virtually no ventilation to these areas, targeted delivery to the maxillary sinus presents an even more formidable challenge than to the olfactory region. As discussed in Si et al a particle released from the nostril tip can go relatively upward to the vicinity of the olfactory region; however, a particle that reaches the maxillary sinus needs to circumvent three obstacles (Figure 1A) and experiences more dramatic direction changes.[32] This challenge could be worse in patients with rhinosinusitis who have blocked ostium, obstructed

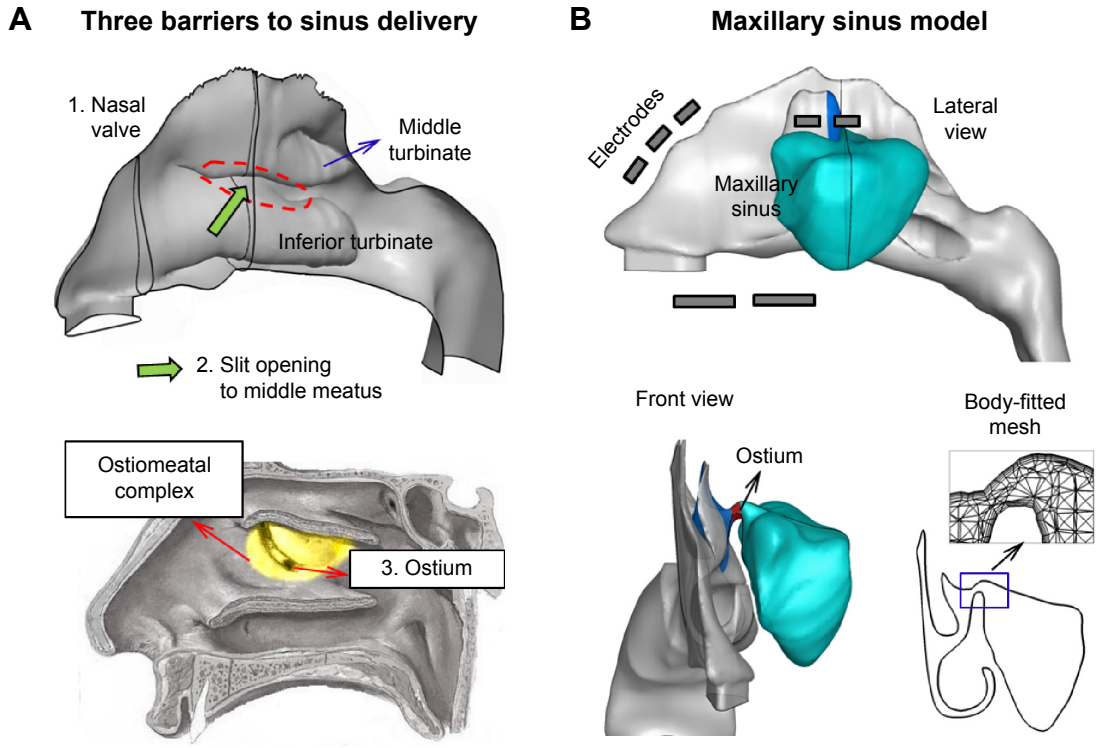

Figure 1 Nose–sinus airway model.
Notes: (**A**) There are three anatomical barriers in the nasal airway preventing effective sinus delivery: 1) the nasal valve, 2) the slit opening to the middle meatus, and 3) the ostium to the maxillary sinus. (**B**) Lateral and front view of the left nasal passage with the ostium and maxillary sinus. A body-fitted mesh is implemented in the near-wall region.

nasal passages, and impaired ventilation due to mucosal swelling or nasal polyps.

The objective of this study is to design a drug delivery system targeting charged particles at the OMC in the nasal MM. The rationale underlying the design is that the path of a charged particle can be controlled by applying appropriate electrical force so that it can escape filtrations and reach the target site. This study has three specific aims: 1) to develop a computational model for nose–sinus drug delivery of charged particles, 2) to determine a baseline design of the delivery system to the OMC region, and 3) to identify the optimal OMC delivery system by refining design variables that are related to the device layout, drug particles, and patient breathing. The particle size considered is ~20 nm, and the electrode potentials are <200 V. The nose–sinus model was constructed from MRI images. The gradient-free Nelder-Mead algorithm was used for the design optimization.

Methods

Nose–sinus model and electric-guided delivery system

MRI scans of a healthy 53-year-old male were used to develop the nose–sinus airway model (Figure 1B). This dataset was initially implemented in 1989 by Guilmette et al to prepare in vitro casts and has been used in multiple simulations and experiments of particle depositions.[33–37] Image-segmentation software MIMICS (Materialise, Ann Arbor, MI, USA) was used to convert the MRI scans into contours defining the nasal cavity and the maxillary sinus. A surface geometry was constructed from these contours in Gambit.

The diagram of the delivery system for charged particles is shown in Figure 1B and will be discussed in detail in Figure 5. The proposed delivery system consists of multiple electrodes positioned around the nose. After a charged particle is released into the nose, an electric force is exerted onto it and makes it depart from its original path. With a proper electric field, the particle can be guided to the target site with reduced deposition in the anterior nose. To further enhance the delivery efficiency, drug particles can be released into the nose from a selected point instead of the entire nostril, that is, point drug release.[23,32] In practice, a vibrating mesh nebulizer can be used to generate submicrometer particles, which acquire electrostatic charges through either induction or corona charging.[38,39] The charged particles subsequently enter a focusing chamber to form a particle beam, which is accelerated to a particular exit speed.[40] The benefit of knowing the particle release velocity is that the particle trajectory can be found, and the path adjustments required for improved depositions can be determined. The target in this study is the

OMC, which hosts the ostium orifice to the maxillary sinus and is where most sinusitis disorders occur.[41]

Study design

Objective function and design constraints

The design objective is to maximize the OMC deposition of charged particles subjected to an external electric field. Due to the complex nasal architecture and the poor ventilation to the MM, only a minor fraction of inhaled air and particles can penetrate into the OMC.

Design constraints in this study are the topological feasibility of the electrode layouts, the range of the electric potential, the electrostatic charge limit of particles, and the spatial constraints of the nozzle exit within the nostril. The shape and size of the nozzle exit are limited by the operational feasibility, which has a rectangular shape and an area of 5.25 mm^2 in this study. The inhalation speed is 0.1 m/s. The particle diameter is 20 nm. The electrode voltage is below 220 V, and the maximal particle charge number is 150, which is 42% of the Rayleigh limit (356.7) for 20 nm particles.[42]

Design variables

There are three categories of design variables: device-related, particle-related, and patient-related. The device-related variables include the drug release position, the nozzle shape, and three electrode groups (E-groups). Among the three E-groups, the first E-group aims to reduce nasal valve filtrations and contains four electrodes, the electric potentials of which are parameterized with B1, T1, T2, and T3. Similarly, the second E-group has one electrode (B2) that facilitates particles to enter the MM through the slit opening, while the third E-group has two electrodes (C1 and C2) to attract particles to the OMC. The point-release position and nozzle shape are parametrized as (x, z, a, and A/a), where A is the nozzle area. The particle-related variables include the density ρ, diameter d_p, and charge number n. The patient-related variable is the inhalation rate, V_{in} (m/s). As a result, there are 14 design variables in total (Table 1).

Process

Design and optimization of the delivery system were performed in a four-step process. First, the required electric fields for effective particle controls were selected using a two-plate channel. Second, a baseline design was devised that gave relatively satisfactory delivery efficiencies, and the key design parameters were identified by means of sensitivity analysis. Third, design variables that are related to the device, particles, and patients were optimized separately with the baseline design as the starting point. Finally, the three categories of design variables were combined to yield the final optimal solution.

Optimization algorithm

The Nelder-Mead algorithm was adopted in this study for its robustness. It is a gradient-free nonlinear optimization technique for problems whose derivatives of the objective function are unknown or very noisy. This algorithm uses the concept of a simplex (a generalized triangle in N dimensions) to control the search direction by comparing the objective function at each test point of the current or triangle. The point that gives the worst result is rejected and replaced with a new vertex, which is the reflection of the centroid of

Table 1 Design variables of the electric-guided delivery system to the ostiomeatal complex

Design variables		Variable	Baseline	Optimization							
				Inlet	E-1	E-2	E-3	d_p	n	V_{in}	Full
Device-related	Inlet (mm)	x	10.2	**10.2**	10.2	10.2	10.2	10.2	10.2	10.2	**10.2**
		z	6.4	**6.1**	6.4	6.4	6.4	6.4	6.4	6.4	**6.1**
		a	1.5	**1.4**	1.5	1.5	1.5	1.5	1.5	1.5	**1.4**
	E-1 (V)	T1	100	100	**172.9**	100	100	100	100	100	**162.3**
		T2	100	100	**171.5**	100	100	100	100	100	**160.8**
		T3	100	100	**64.6**	100	100	100	100	100	**60.8**
		B1	−100	−100	**−97.5**	−100	−100	−100	−100	−100	**−70.2**
	E-2 (V)	B2	100	100	100	**119.7**	100	100	100	100	**102.2**
	E-3 (V)	C1	−150	−150	−150	−150	**−80.1**	−150	−150	−150	**−72.0**
		C2	−150	−150	−150	−150	**−200**	−150	−150	−150	**−205**
Particle-related	Diam (nm)	d_p	20	20	20	20	20	**18.4**	20	20	**24.5**
	Charge (charge number)	n	100	100	100	100	100	100	**109.4**	100	**136.2**
Patient-related	Inhale (m/s)	V_{in}	0.1	0.1	0.1	0.1	0.1	0.1	0.1	**0.092**	**0.117**
OMC delivery (%)			45.0	48.8	53.2	47.0	66.4	49.0	49.4	48.6	72.4
Enhancement (%)			0.0	3.8	8.2	2.0	21.4	4.4	4.4	3.6	27.4

Note: The bold numbers are optimized design variables.

Abbreviations: OMC, ostiomeatal complex; Diam, diameter; E-1, E-group 1; E-2, E-group 2; E-3, E-group 3; T1, top 1; T2, top 2; T3, top 3; B1, bottom 1; B2, bottom 2; C1, cone 1; C2, cone 2; d_p, particle diameter; V_{in}, inhalation velocity.

the remaining points, and the search continues. The process generates a sequence of triangles, which progressively get smaller until converging to the optimal position.

Airflow and particle transport models

Incompressible and isothermal airflow were assumed in this study, with steady inhalations. The inlet Reynolds number at the nostril was ~64; therefore, the laminar flow model was implemented to resolve the airflow field.

Particle trajectories were computed using the Lagrangian tracking scheme. The particle diameter considered in this study was 20 nm. Aerosols in this size range have very low Stokes numbers and particle inertia. The governing equation of particle motions is[43]:

$$\frac{dv_i}{dt} = \frac{c_d}{\tau_p C_c}\left(u_i - v_i\right) + g_i + f_{i,\text{Brownian}} + f_{i,\text{electric}} + f_{i,\text{magnetophoretic}}. \quad (1)$$

The four terms in the right-hand side of the Equation 1 are drag force, particle gravity, Brownian force, electric force, and magnetophoretic force, respectively. Here, v_i is the particle velocity, u_i is the local fluid velocity, c_d is the drag factor, C_c is the Cunningham slip factor, and τ_p is the characteristic time required for a particle to respond to changes in the flow field. The electric force is calculated as:

$$f_{i,\text{electric}} = neE; \qquad E = -\nabla U, \quad (2)$$

where n is the charge number of the particle, E is the electric field intensity, and U is the electrode potential. The elementary charge e is 1.602×10^{-19} C. The governing equation of the magnetic field and magnetophoretic force for a ferromagnetic particle is,

$$B = \mu_0\left(H + M\right); \; F_{i,\text{Magnetophoretic}} = \left(\mu_0 m_{\text{eff}} \times \nabla\right)H. \quad (3)$$

In Equation 3, B is the magnetic flux density, H is the magnetic intensity, M is the magnetization, μ_0 is the permeability of free space, and m_{eff} is the effective magnetic dipole moment. Details of the magnetophoretic force can be found in Xi et al.[30] The simulations were conducted using a finite element analysis software COMSOL (Burlington, MA, USA).

Results

Airflow field, flow partition to the MM, sinus ventilation

Airflow dynamics inside the nose and maxillary sinus is shown in Figure 2. Inhaled air experiences a 90°-bend in the anterior nose, passes through the turbinate regions, and enters a more spacious nasopharynx. Due to the area expansion, a recirculation zone forms in the nasopharynx (left panel, Figure 2A). The MM is the space between the inferior and middle turbinates (middle panel, Figure 2A); due to its distal location, <10% of inhaled air is ventilated into the MM (right panel, Figure 2A). In contrast, >50% of inhaled air passes through the median passage. Even less inhaled air (<0.1%) enters the sinus. Only streamlines originating at the middle outer nostril can penetrate into the maxillary sinus (Figure 2B). Furthermore, there is almost no pressure difference between the OMC and the maxillary sinus. The airflow motion inside the sinus is extremely slow (0.02 cm/s) relative to the flows in the median passage (20 cm/s). A weak flow recirculation is observed inside the sinus (Figure 2C).

Parameter selection

This section explains how design variables and their design spaces were selected. The particle size of the initial design was selected as 20 nm based on its high charge/mass ratio and high sensitivity to electric or magnetic controls. A slow inhalation rate (0.1 m/s) was chosen so that particles can have sufficient time to respond to the electric guidance. The layout of the electrodes was devised to minimize drug waste in regions other than the target. In particular, the selection of the point-release position and electromagnetic field is detailed in Figures 3 and 4, respectively.

Point-release position

The point-release technique has been shown to significantly enhance site-specific drug delivery efficiencies.[32,44] In this study, these positions are identified inversely by tracing all particles that deposit in the sinus back to their original release position (Figure 3A). The logic is that a particle released from this region (blue-dashed rectangle) has a larger chance to penetrate into the sinus. However, as seen in Figure 3B, even from this region, not all particles penetrate into the sinus or MM. Therefore, it is not feasible to achieve meaningful sinus doses by means of the point-release technique. In this test case, 30,000 particles were released into the entire nostril. Only 29 particles (~0.1%) succeeded in depositing into the sinus (Figure 3B). This ratio is too low to be useful for clinical purposes. Moreover, 99.9% particles deposit on the walls other than the targeted sinus and can cause severe adverse side effects. New techniques that can dramatically increase the sinus doses and minimize wastes in other regions are needed for effective and efficient treatments of acute and chronic rhinosinusitis.

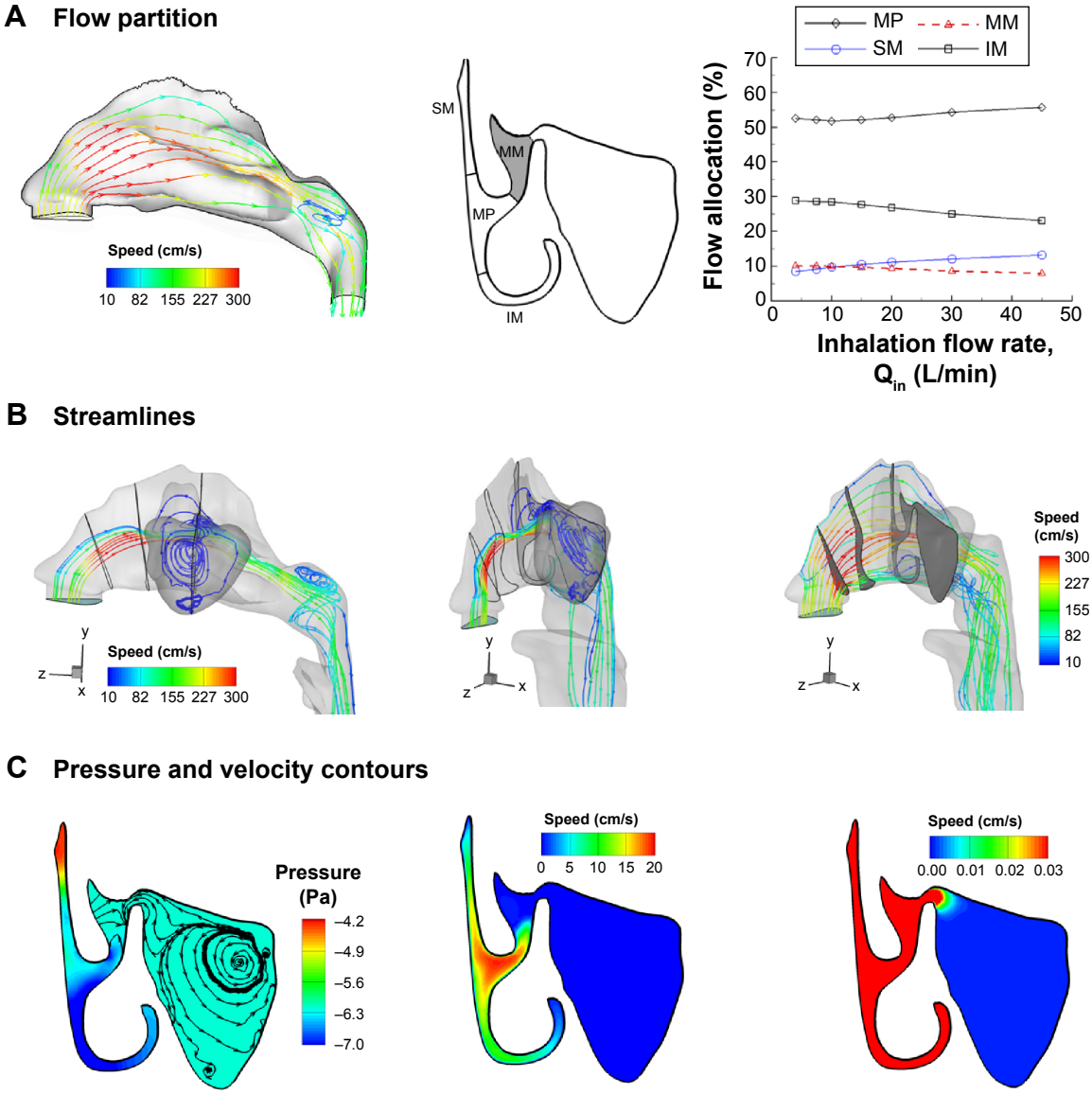

Figure 2 Airflow dynamics in the nasal-sinus airway.
Notes: (**A**) <10% of inhaled air is ventilated into the middle meatus. (**B**) Even less portion (<0.1%) of inhaled air is ventilated into the sinus. Only airflows originated at the middle outer nostril can possibly enter the sinus; airflows originated at other regions will pass through the median passages of the nose. (**C**) There is almost no pressure difference between the ostium and sinus. The airflow motion inside the sinus is extremely slow relative to the flows in the main nasal chamber.
Abbreviations: SM, superior meatus; MM, middle meatus; MP, median passage; IM, inferior meatus.

In this study, the nozzle exit was chosen to be a rectangle with a fixed area of 5.25 mm^2 (Figure 3A). The position and shape were parametrized by the inlet center coordinates (x, z) and the inlet length a (the width b=5.25/a [mm]). The orientation of the inlet is parallel to the lateral wall of the nostril and is 25° from the positive z-direction (Figure 3A).

Electromagnetic field

The selection of the magnitude of electrodes and magnets is illustrated in Figure 4. Based on an inlet velocity of 0.1 m/s, a particle size of 20 nm, and a charge number of 100, the required electric field strength for effective particle control can be theoretically obtained. By using Equations 1 and 2, the required electric field strength is calculated as 2.6×10^{-3} V/m for gravity equivalence and is 250 V/m for particle inertia equivalence. With a characteristic length of 20 mm for the human nose, the required electrode differential voltage is 5 V, which is much smaller than 220 V. The electrode potentials in the range of 5–220 V were subsequently tested in a two-plate channel with a height of 20 mm and a length of 200 mm. From Figure 4A, we can observe that there are perceivable trajectory modifications when particles are subjected to an external electric potential of 8 V. The trajectory modification is more pronounced when E =20 V (Figure 4A).

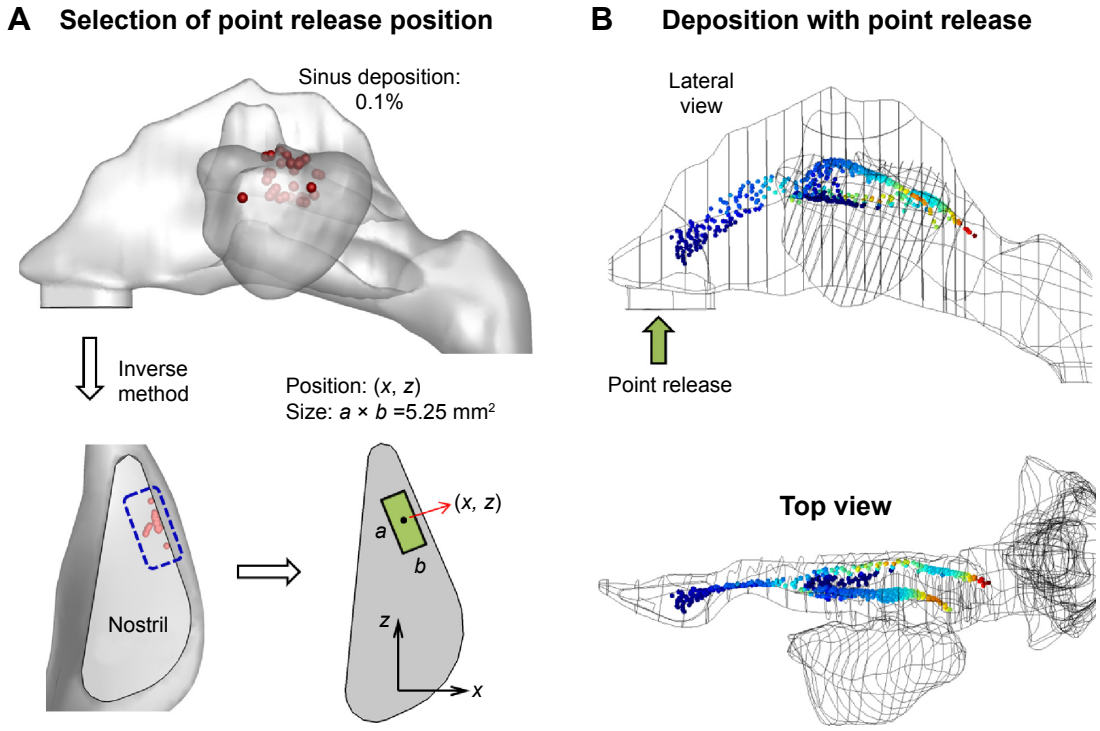

Figure 3 Point-release position and particle deposition.
Notes: (**A**) Selection of point-release position using an inverse method and (**B**) the resultant particle surface deposition without electric guidance. Particles that deposit in the sinus are traced back to their initial-release position. Particles introduced from the rectangle have more chances to enter the sinus. The area of the rectangle is fixed at 5.25 mm², while the width and length (a × b) can change. An extremely low fraction of inhaled particles (0.1%) deposits in the sinus.

Once the particle size, inlet velocity, and electric potential were selected, further tests were conducted to see if a magnetic force could be added for more precise control of particle motions. The mutually orthogonal electric and magnetic forces on a charged particle in an electromagnetic field offer a potential of two-dimensional control on particle trajectories. For particles that reach the OMC (outside the sinus), it is especially desirable to further guide them into the sinus by applying a magnetic force normal to the direction of particle motion. Three magnitudes of magnification were

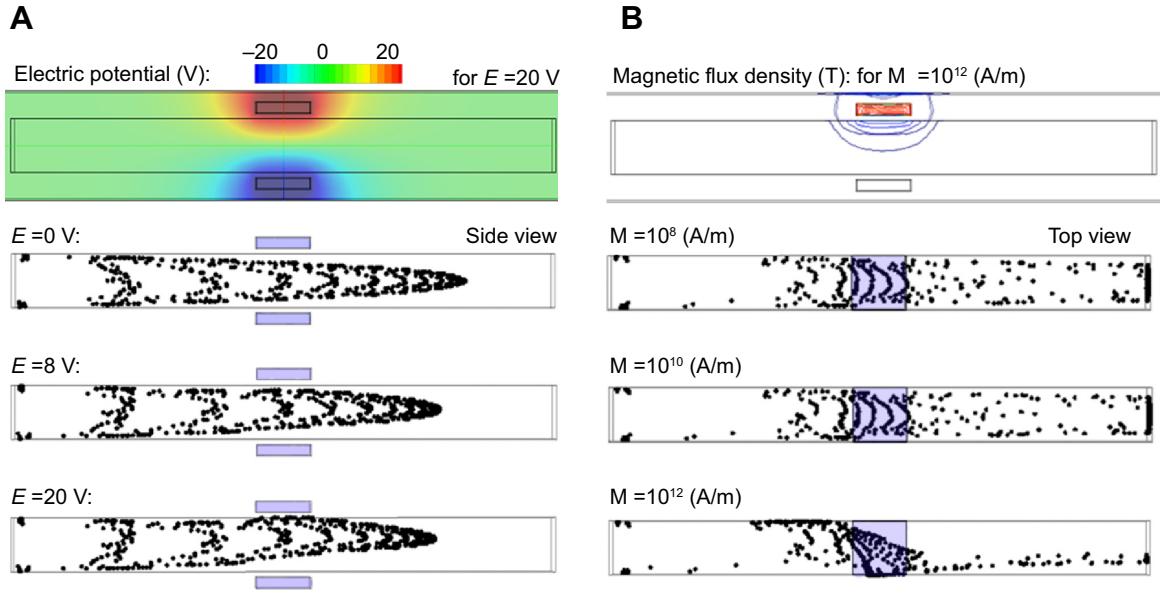

Figure 4 Parameter selection for electric and magnetic fields applicable to the design of a paranasal delivery system.
Notes: (**A**) Electric field, and (**B**) magnetic field.
Abbreviation: M, magnetization.

tested for this purpose, and the results are shown in Figure 4B. No discernible response of particle motion was observed for the magnetization of 1×10^8 A/m and 1×10^{10} A/m, while substantial course changes were observed when $M=1\times10^{12}$ A/m. Considering that the commonly available magnetization strength is 10^8 A/m or smaller (eg, a neodymium magnet), the required magnet strength (1×10^{12} A/m) is too high to be feasible in this study.[45] As a result, only electric force was used in the subsequent design and optimization of the sinus delivery system.

Baseline design

There are two stages in designing the delivery system: 1) development of a baseline design and 2) optimization of the delivery protocol. Figure 5A shows the electrode layout of the baseline model. This model was obtained based on the selected design spaces after a large number of trials and errors. There are seven electrodes around the nose, which are divided into three groups according to their designated functions (Table 1). To guide a particle into the MM that otherwise passes through the median passage, a different path (blue line) from the aerodynamically driven trajectory (red line) should be followed, as shown in Figure 5B. The particle should first move downward to avoid entering the median passage and then move upward to enter the MM through the slit-opening between the inferior and middle turbinates. The first group consists of four electrodes (B1, T1, T2, and T3) and aims to shift the trajectories of inhaled particles both downward and sideways (Figure 5B). The downward motion helps to reduce the nasal valve filtration by allowing the majority of particles passing through the wider, lower part of the nasal valve (upper panel, Figure 5B). The sideways motion will help the particles to deviate from the main airstream and turn to the MM (lower panel, Figure 5B). The second group consists of only one electrode (B2), which is intended to push the particles toward the slit opening of the MM. A precise control of particle motion in the lateral direction is necessary for optimal delivery efficiency considering the slim slit opening. A slight oversteering to the median will increase particle losses to the mucosa of the middle turbinate, and an understeering will increase losses to the nasal lateral surface. The third E-group comprises two cone-shaped electrodes (Figure 5A), which are positioned close to the ostium to concentrate particles into the ostium opening.

The electric field of the baseline delivery system is shown in the lower panel of Figure 5A. The resultant delivery efficiency to the OMC is shown in Figure 5C. In comparison with that without E-guidance, this proposed system significantly improves the OMC delivery, that is, from 0.1% to 45.0% (Figure 5C). However, there are still a considerable amount of particles wasted in the nasal valve (dashed ellipse) and the MM opening (red circle, Figure 5C). In addition, some particles pass the OMC but do not deposit there (red arrow in Figure 5C). As a result, further improvements to the baseline delivery system are still possible by minimizing drug losses in the abovementioned three regions.

Sensitivity analysis of design variables

Sensitivity analysis was conducted to examine the effects of individual parameters and identify key design variables (Figure 6). Each variable was tested by varying ±10% of the baseline value, and the result was shown as the percent change from the baseline OMC dosage. Different levels of sensitivity of the OMC deposition to the design variables were observed. It was highly sensitive to the inhalation rate, particle diameter, charge number, and electrode potential above the sinus ostium (C1). On the other hand, the influences of both inlet and the top electrodes (T2 and T3) are observed to be much smaller. This low sensitivity of the two top electrodes can presumably be explained by their indirect influence on the OMC dosage. It is also observed that B1, which lowers the particles in the valve region, exerts a much larger impact on OMC dosages than B2, which drives particles upward into the MM. No influence was observed from the particle density within the test range (±10%).

Single-component optimizations

Optimization of particle release position

In order to find the best efficiency, all design components listed in Figure 6 were optimized except the particle density. Optimization of the center of the drug-release nozzle (x, z) is shown in Figure 7. The nozzle is positioned at the nostril and has a rectangular shape and a fixed area of 5.25 mm^2 (Figure 3). Figure 7A displays the 3-D plot of the objective functions versus the release position. The Nelder-Mead algorithm explored different points in the design space, which gave different OMC doses and identified the optimal point after 24 steps. The optimization process is also illustrated in Figure 7B with multiple triangles (or simplexes), which progressively shrink in size and converge to the optimal point. At each step, the objective functions of the three points were compared, and the worst was replaced with a new point that was determined by the Nelder-Mead algorithm (Figure 7B). The optimization process stopped when the difference among the objectives is $<$1e-5.

Figure 7C shows the resultant deposition patterns with the optimized release position. Compared with that of the

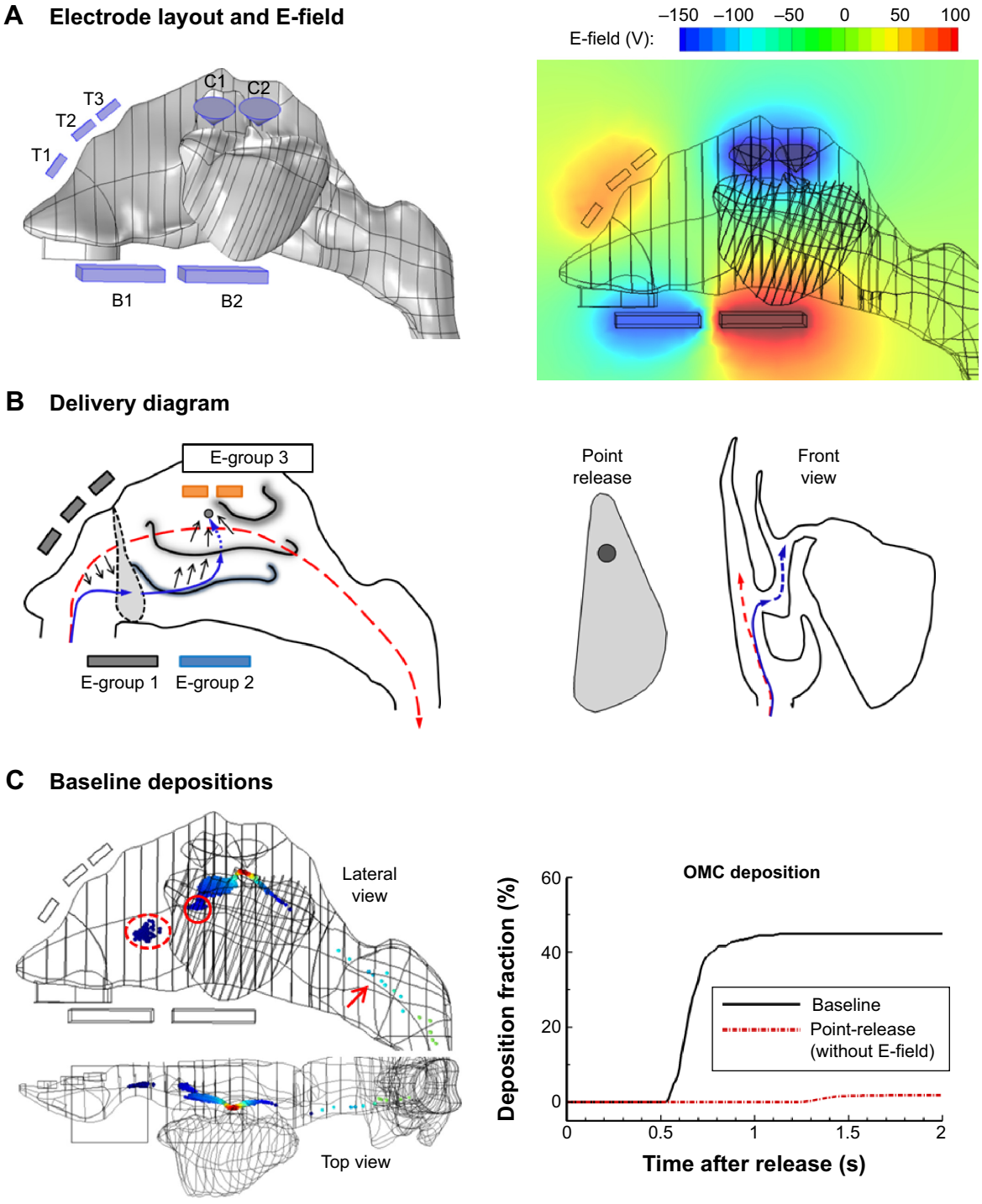

Figure 5 Electrode layout and performance of a baseline design.
Notes: (**A**) Diagram of the electrode layout with three groups and the electric potential field; (**B**) desirable path of particles for effective OMC delivery, and (**C**) depositions with the baseline delivery system. Each electrode group in the proposed delivery system has a designated function. E-group 1 aims to reduce drug deposition in the nasal valve, E-group 2 aims to push particles into the middle meatus, and E-group 3 aims to attract particles to the sinus ostium. Point-release was used to minimize drug loss in regions other than the target.
Abbreviations: OMC, ostiomeatal complex; T, top; B, bottom; C, cone.

baseline model in Figure 5C, particle depositions in the nasal valve and frontal middle turbinate are noticeably reduced. By optimizing the release position, the OMC deposition is increased from 45.0% in the baseline model to 48.8% (Figure 7B).

Optimization of other design variables

Single-component optimizations were conducted in three categories: device-, particle-, and patient-related factors. The device-related factor is further divided into four components: inlet, E-group 1, E-group 2, and E-group 3, as listed

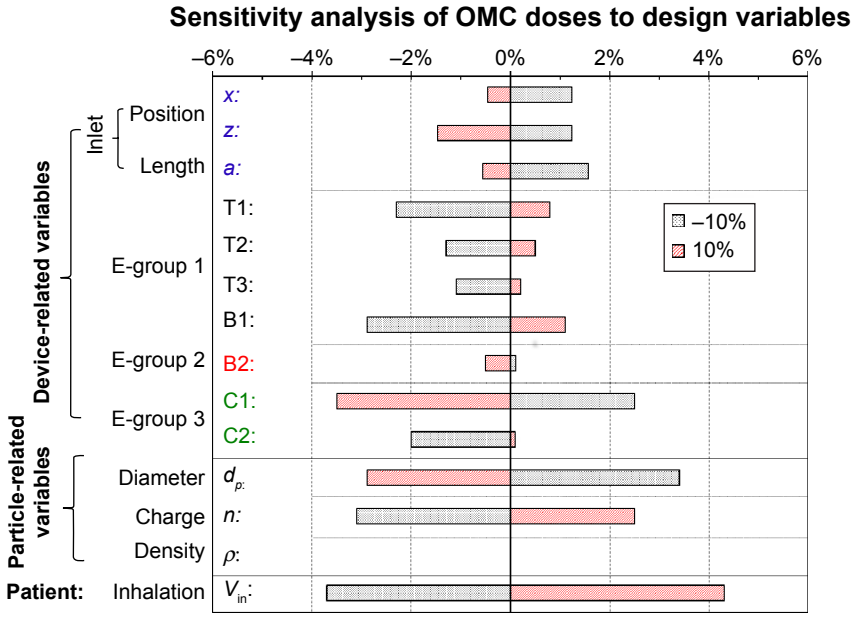

Figure 6 Sensitivity analysis of design variables influencing the OMC delivery efficiency.
Notes: There are 14 design variables in total, which fall into three categories: device-related, particle-related, and patient-related. Each variable was varied by ±10% of the baseline value. The sensitivity results are shown as the percent change from the baseline OMC dose.
Abbreviation: OMC, ostiomeatal complex.

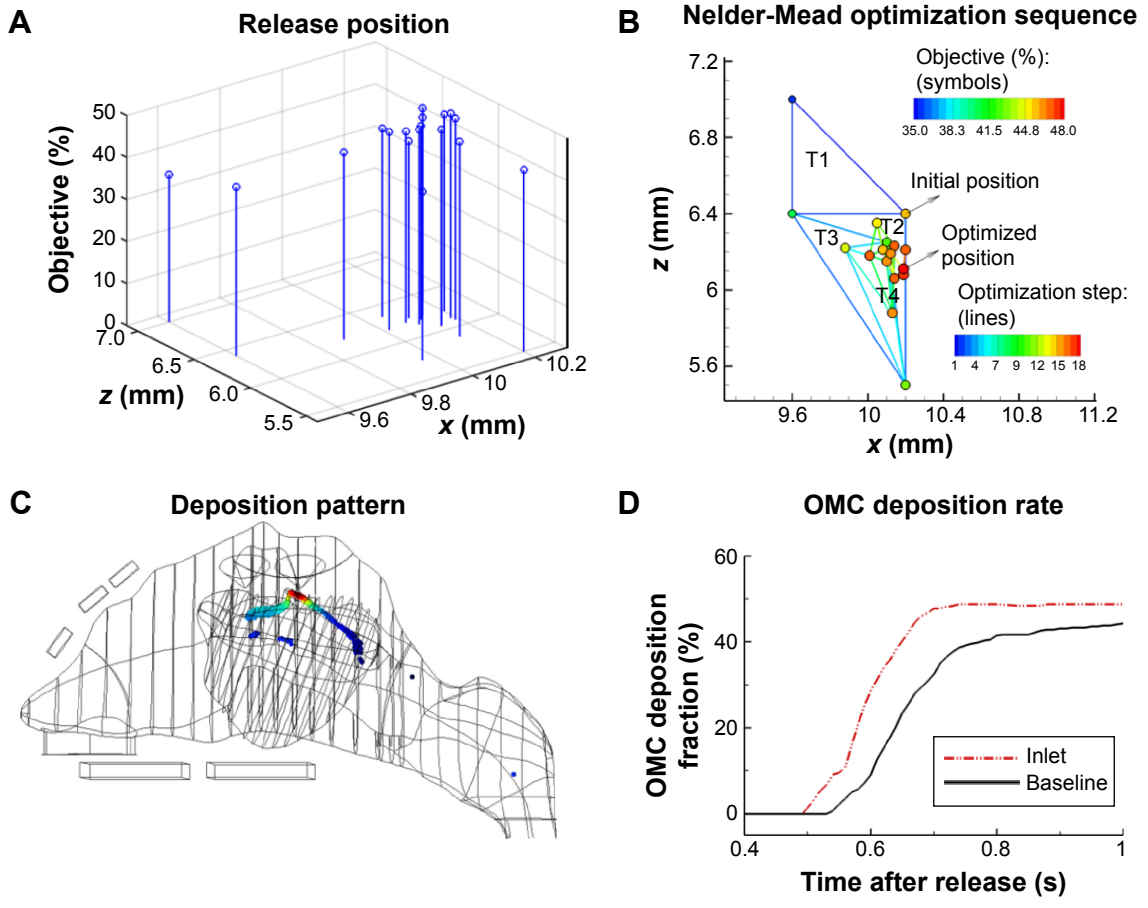

Figure 7 Optimization of the release position (*x*, *z*) at the nostril inlet.
Notes: (**A**) The objective (ie, OMC dose) as a function of the release position, (**B**) the Nelder-Mead optimization sequence with triangles (T_k) converging to the point (10.2, 6.1 [mm]), (**C**) particle deposition pattern with the optimized inlet position, and (**D**) the time evolution of olfactory deposition for OMC deposition with and without inlet-position optimization.
Abbreviations: OMC, ostiomeatal complex; s, seconds.

in Table 1. The particle-related factor has two components: particle diameter and charge number, while the patient-related factor has one component only (inhalation velocity). Surface deposition pattern of each optimized component is shown in Figure 8A. In comparison with the baseline model, E-group 1 successfully eliminated the nasal valve deposition. However, there was still a considerable amount of particles in the middle turbinate (red arrow, E-group 1, Figure 8A). By optimizing E-group 2, the deposition in the middle turbinate was perceivably reduced, but some depositions in middle turbinate still remained. In particular, more particles were observed eluding the OMC filtration and escaping into the nasopharynx (red arrow, E-group 2, Figure 8A). In contrast, by optimizing the E-group 3 (the two cones), particle loss into the nasopharynx was greatly reduced; however, the nasal valve deposition increased (red arrow, E-group 2, Figure 8A). It is noted that it is the synthesis of design variables, not one individual variable, which determines the delivery efficiency to the target. Deposition patterns of particle- and patient-related components are shown in Figure 8B and C. Noticeable improvements were observed for each component relative to the baseline model.

Comparison of the OMC delivery efficiency among optimized components is shown in Figure 8D and Table 1. Different levels of delivery enhancements were achieved from various components. The E-group 3 gave the largest dosage increase (21.4%), while the E-group 2 gave the least (2.0%). The E-group 1 gave the second largest dose increase (8.2%). Optimizations of particle-related (d_p and n) and patient-related (V_{in}) components, as well as the inlet, only gave moderate improvements (3.6%–4.4%). This result does not contradict the previous results from the sensitivity analysis as presented in Figure 6, which varies the variable magnitude by ±10%. In contrast, the optimization design variables can vary in a much wider range. For instance, the position of the release point is highly constrained by the nostril orifice, while the electrode potentials are only loosely limited by a practical voltage (220 V in this study). As a result, the electrode optimization leads to the major improvement due to their larger allowable design space compared with the other variables. Moreover, some variables influence the OMC delivery in a highly nonlinear manner, such as the inlet velocity, particle diameter, and charge number, and only induce limited dose increase.

Multiple-component optimization: efficiency, surface deposition, merits, and weakness

Effective drug delivery to the OMC depends on the synergy of many factors. Single-component optimization can underestimate the optimal dosages. A full optimization was performed by considering all the three categories of design factors simultaneously. The computational time in this scenario was 148 hours using a 3.2 GHz Dell Precision workstation.

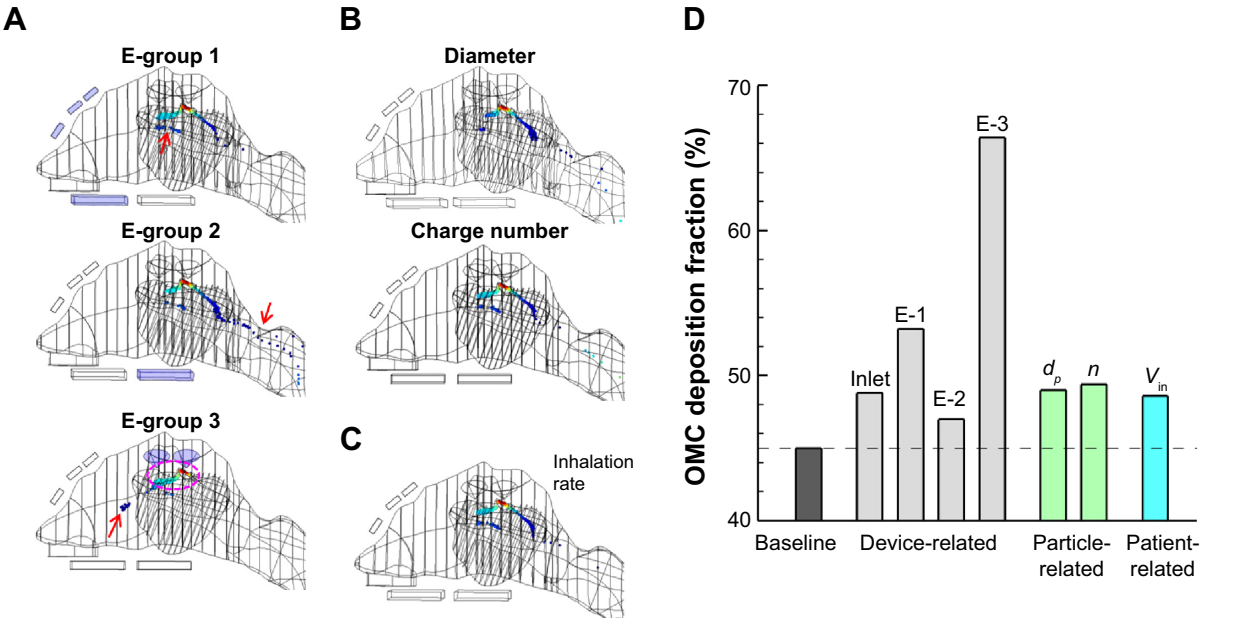

Figure 8 Particle deposition patterns with single-component optimizations.
Notes: (**A**) Device-related, (**B**) particle-related, and (**C**) patient-related components. The comparison of OMC delivery efficiency among single-component optimizations is shown in (**D**).
Abbreviations: E-1, E-group 1; E-2, E-group 2; E-3, E-group 3; OMC, ostiomeatal complex.

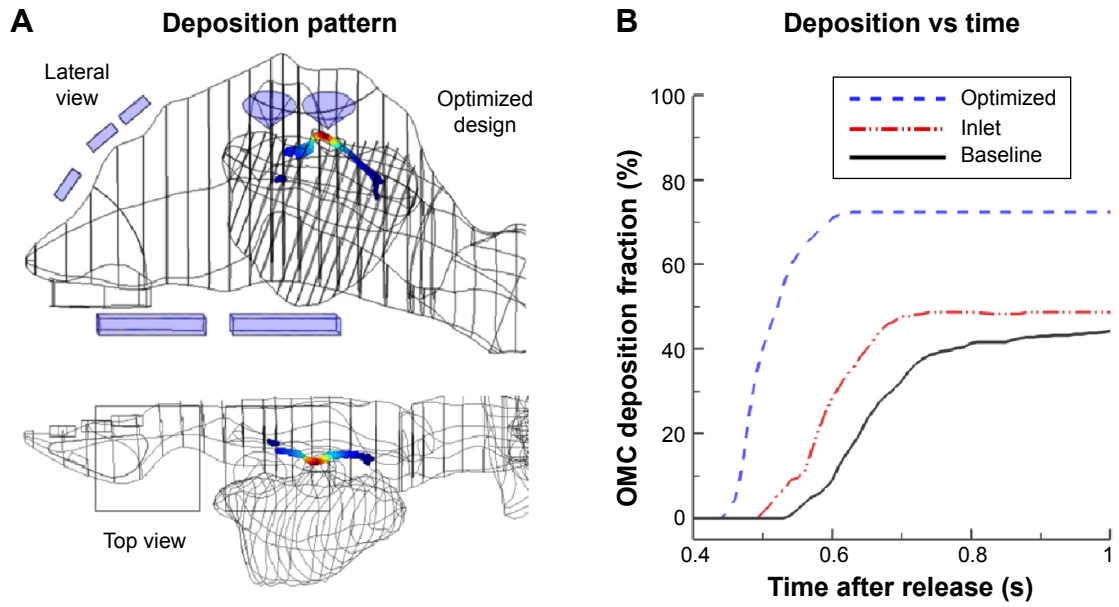

Figure 9 Deposition with optimized design.
Notes: (**A**) Particle deposition pattern, and (**B**) time evolution of OMC depositions.
Abbreviations: OMC, ostiomeatal complex; s, seconds.

Figure 7 shows the results of the baseline and optimized designs, with the optimized design variables listed in Table 1. From Figure 9, a 27.4% increase in OMC delivery efficiency was achieved in the optimal design (72.4%) relative to the baseline model (45.0%). The drug loss in the turbinate regions was significantly reduced. In particular, depositions in the nasal valve were entirely avoided (Figures 9A vs 5C). Depositions of drug particles in the optimal design are more focused than those in the baseline model (Figures 9A vs 5C).

Discussion

An optimization framework was presented for the development of targeted delivery system to the OMC with charged nanoparticles. An electric-guided OMC delivery system was proposed based on the unique paranasal structures and was numerically assessed of its performance in a realistic nose–sinus model geometry. The design variables of the abovementioned system (baseline) were further optimized, which included the device layout, particle physical properties, and patient inhalation rates. The OMC delivery efficiency increased from the baseline performance of 45.0%–72.4% with the optimized delivery system. Compared with standard nasal devices such as nasal sprays and pumps, the new delivery system almost eliminated the drug loss in the nasal valve region. Compared with the pulsating aerosol delivery approaches, the new system has the promise to deliver ten times greater doses to the paranasal sinuses.

The most desirable feature of the newly proposed delivery system is its capability to precisely target medications to the OMC, where turbinate mucosal swelling and ostium blockage occur during a sinusitis episode. This is achieved by the synergy of two separate approaches: particle point-release and control of particle motion using electric force. Results of this study demonstrated highly focused particle deposition in the OMC, particularly around the sinus ostium. This focused dose will have the benefits of quicker onset of action, lower systemic side effects, and being more efficacious at lower doses.[46,47] More and more studies have demonstrated that the dosage at the diseased site, rather than the total dose, should be used as the predictor of clinical outcomes.[48] In addition, the initial site of drug deposition has an important effect on its bioavailability and associated therapeutic effectiveness.[49]

Another advantage of the newly proposed delivery system is its versatility. Drug particles under the control of an electric field are less dependent on inhalation conditions, which makes the proposed device well suited to be used by children, seniors, or patients with difficulties in following the instructed breathing maneuvers.[50,51] This advantage is especially desirable when medications need to be administered over a sustained period of time. Furthermore, depending on the needs, the proposed device can be readily adapted to deliver drugs either to other regions of the nasal airway, for a different patient, or with drugs of different physical properties (density, size, electrostatic charge, etc). This can be achieved by adjusting the external electric field and breathing conditions specific to that need through the design and optimization as outlined in this study. A delivery device based on this proposed system is intended to be patient-specific, which utilizes

the patient's MRI scans to determine the design variables. It can also be used for generic purposes; however, the delivery efficiency will be reduced considering the intersubject variability in nasal anatomy and physiology. In this scenario, uncertainty analysis is needed to quantify the performance variances across a broad spectrum of patients.[52]

It is also noted that the newly proposed delivery system is capable of targeting drugs at the OMC, not the maxillary sinus itself. With this system, particles cannot enter the sinus due to the secluded location and long, narrow canal shape of the ostium that connect the OMC and sinus. Other studies have demonstrated the feasibility of delivering aerosolized medications (1%–5%) into the sinus with the help of pulsating flows.[3,9–12] Even though the maxillary sinus is a closed hollow organ, Hyo et al observed aerosol flows within it when a pressure gradient was applied between the nasal cavity and the maxillary sinus.[53] Based on the observation that humming can induce rapid gas exchanges, Maniscalco et al reported more homogeneous distributed particles in the nasal cavity.[11] Using a pulsating flow with 100 Hz frequency, Durand et al measured an increase of particle deposition into the sinus by a factor of five.[12] It is suggested that by combining the electric-guided protocol with a pulsating flow, more particles can be delivered into the maxillary sinus, with particle transport to the OMC by electric guidance and into the sinus by acoustic waves. The electric guidance and acoustic flows act independently on particle motions and do not interfere with each other. Future studies on delivery systems with both electric and acoustic controls are needed.

In practice, the delivery system will comprise two electrodes within the mouth, three electrodes above the anterior nose, and two electrodes outside the maxillary sinus (Figure 5A). As all electrodes will be outside the body, no surgery is needed in this application. These seven electrodes belong to three groups according to their designated functions and together generate an expected electric field inside the nasal cavity. While high voltages (up to 220 V) are used in the electrodes, the current in them is zero. The electrodes are covered with plastic that negligibly affects the field strength while safely keeping the patient from contacting the voltage source.

The design of the proposed delivery system was based on the nasal airway of a healthy subject. In patients with sinusitis, airway obstruction and sinus ostium blockage caused by the mucosal inflammation lead to more impaired ventilations in the nasal passage and sinus. As a result, it will be more challenging to deliver drugs to the OMC in patients with sinusitis. Modifications of electrode strengths are needed to adapt to the required particle trajectories in patients with sinusitis versus healthy subjects. For severely obstructed airways, decreased OMC delivery doses are expected. Furthermore, therapeutic particles might not enter the maxillary sinus when the diameter of the sinus ostium canal is <1 mm.[53] To address these abovementioned challenges, vasoconstrictors can be applied to the patient to ease the airway obstruction before administering therapeutic agents.

Water droplets were tested in this study. Other nasal formulations can also be considered to further improve the OMC dosage or enhance medication absorption rate. For instance, nasal sprays with low-viscosity formulations give greater coverage of the nasal surface than high-viscosity formulations.[54] In contrast, high-viscosity formulations can be used to achieve more focused delivery with reduced drug dispersion. Once a particle is trapped in the nasal mucosa, it will be either removed by mucociliary clearance or dissolved and absorbed by the underlying tissue. Adding bioadhesive polymers into nasal sprays prolongs the drug residence time and helps to survive the mucociliary clearance.[55] One example is microcrystalline cellulose, which has been commonly used as an absorption enhancer for the treatment of allergic rhinitis.[56]

A gradient-free algorithm has to be used, and the computational time increases exponentially with the number of design variables.[57] For an optimization with two variables (eg, the inlet position), the optimization required 35–50 steps and took about 26−38 hours with a 3.2 GHz Dell Precision workstation. This study optimized 14 design variables. The computational time could be prohibitive if the design optimization started from an arbitrary model or with an open design space. In order to reduce the computational time for optimization, a baseline delivery system with relative satisfactory performance should be used as a starting point. Furthermore, single-component optimization was performed for each key factor to narrow down the design space before multiple-component optimization with all design variables was conducted. The final optimization took 148 hours using a 3.2 GHz Dell Precision workstation.

Some assumptions may influence the realism of the predictions in this study, which include steady inhalations, rigid surface, one particle size, limited electrode layouts, and numerical modeling only. A low inlet velocity (0.1 m/s) was used to decrease the particle inertia and maximize the particle response time to electric forces. Breath holding can also be an alternative to the slow inhalation. The reason underlying the selection of slow inhalation over breath holding herein was that a reference streamline was needed to determine the E-potentials to steer a particle from the reference path to the designated path. The uncertainties

of delivery efficiencies related to breathing variations can be mitigated by telling patients to breathe steadily and by administering drugs only during the steady phase. In this study, 20 nm particles were considered based on their high charge/mass ratio and associated high sensitivity to extremal electric controls. For other particle sizes, a different set of design variables may be needed to give optimal delivery efficiency. The layout of electrodes can be affected by the facial topology and naso–oral anatomy. Additionally, the nose–sinus model in this study was based on medical images of one subject and therefore cannot account for the inter-subject variability. Future numerical studies with a larger cohort of image-based nose models as well as experimental validations are needed to assess the performance of this drug delivery technique.

Conclusion

In summary, a delivery system for the topical treatment of rhinosinusitis was developed to target charged nanoparticles at the OMC. Its performance was numerically tested in an image-based nose–sinus model geometry and was optimized in terms of the device-, particle-, and patient-related design variables. Specific findings of this study are as follows:

1) The electric-guided delivery system shows promising results of significantly higher OMC dose than standard nasal devices.
2) With optimized electric control and point drug release, an OMC delivery efficiency of 72.4% can be achieved.
3) The OMC delivery system exhibits high sensitivity to the applied electric field and particle electrostatic charges but is relatively insensitive to the density of the particle.
4) Due to the large number of design variables, optimization is imperative to achieve a sound delivery protocol. The OMC dose increased from 45.0% in the baseline model to 72.4% in the optimized design.
5) The OMC delivery system can be readily adapted for drug delivery to other regions in the nose, for a different patient, or with drugs of different physical properties.

Acknowledgments

This study was funded by Central Michigan University Innovative Research Grant P421071 and Early Career Award P622911. Jensen Xi, Zachary Firlit, and Alyssa Soltis are gratefully acknowledged for reviewing the paper. We also thank Ze Zhang for technical supports in modeling.

Disclosure

The authors report no conflicts of interest in this work.

References

1. Laube BL. Devices for aerosol delivery to treat sinusitis. *J Aerosol Med*. 2007;20(suppl 1):S5–S18.
2. Baumann I, Blumenstock G, Zalaman IM, et al. Impact of gender, age, and comorbidities on quality of life in patients with chronic rhinosinusitis. *Rhinology*. 2007;45(4):268–272.
3. Möller W, Schuschnig U, Celik G, et al. Topical drug delivery in chronic rhinosinusitis patients before and after sinus surgery using pulsating aerosols. *PLoS One*. 2013;8(9):e74991.
4. Huang S-F, Lee T-J, Lin K-L. Concomitant bilateral orbital and brain abscesses – unusual complications of pediatric rhinosinusitis. *Chang Gung Med J*. 2005;28(1):51–55.
5. Harbo G, Grau C, Bundgaard T, et al. Cancer of the nasal cavity and paranasal sinuses – a clinico-pathological study of 277 patients. *Acta Oncol*. 1997;36(1):45–50.
6. Selam J-L. Inhaled insulin: promises and concerns. *J Diabetes Sci Technol*. 2008;2(2):311–315.
7. Djupesland PG, Skretting A, Winderen M, Holand T. Bi-directional nasal delivery of aerosols can prevent lung deposition. *J Aerosol Med*. 2004; 17(3):249–259.
8. Djupesland PG. Nasal drug delivery devices: characteristics and performance in a clinical perspective-a review. *Drug Deliv Transl Res*. 2013;3(1):42–62.
9. Leclerc L, Pourchez J, Aubert G, et al. Impact of airborne particle size, acoustic airflow and breathing pattern on delivery of nebulized antibiotic into the maxillary sinuses using a realistic human nasal replica. *Pharm Res*. 2014;31(9):2335–2343.
10. Möller W, Schuschnig U, Bartenstein P, et al. Drug delivery to paranasal sinuses using pulsating aerosols. *J Aerosol Med Pulm Drug Deliv*. 2014;27(4):255–263.
11. Maniscalco M, Sofia M, Weitzberg E, Lundberg JO. Sounding airflow enhances aerosol delivery into the paranasal sinuses. *Eur J Clin Invest*. 2006;36(7):509–513.
12. Durand M, Pourchez J, Aubert G, et al. Impact of acoustic airflow nebulization on intrasinus drug deposition of a human plastinated nasal cast: new insights into the mechanisms involved. *Int J Pharm*. 2011;421(1):63–71.
13. Cankurtaran M, Celik H, Coskun M, Hizal E, Cakmak O. Acoustic rhinometry in healthy humans: accuracy of area estimates and ability to quantify certain anatomic structures in the nasal cavity. *Ann Otol Rhinol Laryngol*. 2007;116(12):906–916.
14. Wilson IB. The deposition of charged particles in tubes, with reference to the retention of therapeutic aerosols in the human lung. *J Colloid Sci*. 1947;2(2):271–276.
15. Bailey AG, Hashish AH, Williams TJ. Drug delivery by inhalation of charged particles. *J Electrostat*. 1998;44(1–2):3–10.
16. Wong J, Chan H-K, Kwok PCL. Electrostatics in pharmaceutical aerosols for inhalation. *Ther Deliv*. 2013;4(8):981–1002.
17. Yu CP. Theories of electrostatic lung deposition of inhaled aerosols. *Ann Occup Hyg*. 1985;29(2):219–227.
18. Ferin J, Mercer TT, Leach LJ. The effect of aerosol charge on the deposition and clearance of TiO2 particles in rats. *Environ Res*. 1983;31(1): 148–151.
19. Ali M, Reddy RN, Mazumder MK. Electrostatic charge effect on respirable aerosol particle deposition in a cadaver based throat cast replica. *J Electrostat*. 2008;66(7–8):401–406.
20. Scheuch G, Gebhart J, Roth C. Uptake of electrical charges in the human respiratory tract during exposure to air loaded with negative ions. *J Aerosol Sci*. 1990;21(suppl 1):S439–S442.
21. Azhdarzadeh M, Olfert JS, Vehring R, Finlay WH. Effect of electrostatic charge on oral-extrathoracic deposition for uniformly charged monodisperse aerosols. *J Aerosol Sci*. 2014;68(0):38–45.
22. Xi J, Si X, Longest W. Electrostatic charge effects on pharmaceutical aerosol deposition in human nasal-laryngeal airways. *Pharmaceutics*. 2014;6(1):26–35.
23. Ali M, Mazumder MK, Martonen TB. Measurements of Electrodynamic Effects on the Deposition of MDI and DPI Aerosols in a Replica Cast of Human Oral-Pharyngeal-Laryngeal Airways. *J Aerosol Med Pulm Drug Deliv*. 2009;22(1):35–44.

24. Melandri C, Tarroni G, Prodi V, De Zaiacomo T, Formignani M, Lombardi CC. Deposition of charged particles in the human airways. *J Aerosol Sci*. 1983;14(5):657–669.
25. Balachandran W, Machowski W, Gaura E, Hudson C. Control of drug aerosol in human airways using electrostatic forces. *J Electrostat*. 1997;4(0–1):579–584.
26. Hashish AH, Bailey AG, Williams TJ. Selective deposition of pulsed charged aerosols in the human lung. *J Aerosol Med*. 1994;7(2): 167–171.
27. Ali M. Engineered aerosol medicine and drug delivery methods for optimal respiratory therapy. *Respir Care*. 2014;59(10):1608–1610.
28. Xi J, Si X, Gaide R. Electrophoretic particle guidance significantly enhances olfactory drug delivery: a feasibility study. *PLoS One*. 2014; 9(1):e86593.
29. Dames P, Gleich B, Flemmer A, et al. Targeted delivery of magnetic aerosol droplets to the lung. *Nat Nanotechnol*. 2007;2(8):495–499.
30. Xi J, Zhang Z, Si X. Improving intranasal delivery of neurological nanomedicine to the olfactory region using magnetophoretic guidance of microsphere carriers. *Int J Nanomedicine*. 2015;10:1211–1222.
31. Xi J, Zhang Z, Si X. Optimization of magnetophoretic-guided drug delivery to the olfactory region in human noses. *Biomech Model Mechanobiol*. 2015. [under review].
32. Si X, Xi J, Kim J, Zhou Y, Zhong H. Modeling of release position and ventilation effects on olfactory aerosol drug delivery. *Respir Physiol Neurobiol*. 2013;186(1):22–32.
33. Guilmette RA, Wicks JD, Wolff RK. Morphometry of human nasal airways in vivo using magnetic resonance imaging. *J Aerosol Med*. 1989;2(4):365–377.
34. Cheng KH, Cheng YS, Yeh HC, Swift DL. Deposition of ultrafine aerosols in the head airways during natural breathing and during simulated breath-holding using replicate human upper airway casts. *Aerosol Sci Technol*. 1995;23(3):465–474.
35. Kelly JT, Asgharian B, Kimbell JS, Wong B. Particle deposition in human nasal airway replicas manufactured by different methods. Part I: inertial regime particles. *Aerosol Sci Technol*. 2004;38:1063–1071.
36. Schroeter JD, Kimbell JS, Asgharian B. Analysis of particle deposition in the turbinate and olfactory regions using a human nasal computational fluid dynamics model. *J Aerosol Med*. 2006;19(3):301–313.
37. Xi J, Berlinski A, Zhou Y, Greenberg B, Ou X. Breathing resistance and ultrafine particle deposition in nasal-laryngeal airways of a newborn, an infant, a child, and an adult. *Ann Biomed Eng*. 2012;40(12): 2579–2595.
38. Covert D, Wiedensohler A, Russell L. Particle charging and transmission efficiencies of aerosol charge neutralizers. *Aerosol Sci Technol*. 1997; 27(2):206–214.
39. Golshahi L, Longest PW, Holbrook L, Snead J, Hindle M. Production of highly charged pharmaceutical aerosols using a new aerosol induction charger. *Pharm Res*. 2015;31:31.
40. Zeng Y, von Klitzing R. Scaling of layer spacing of charged particles under slit-pore confinement: an effect of concentration or of effective particle diameter? *J Phys Condens Matter*. 2012;24(46):464125.
41. Rawlings BA, Higgins TS, Han JK. Bacterial pathogens in the nasopharynx, nasal cavity, and osteomeatal complex during wellness and viral infection. *Am J Rhinol Allergy*. 2013;27(1):39–42.
42. Marginean I, Znamenskiy V, Vertes A. Charge reduction in electrosprays: slender nanojets as intermediates. *J Phys Chem B*. 2006;110(12): 6397–6404.
43. Xi J, Longest PW. Transport and deposition of micro-aerosols in realistic and simplified models of the oral airway. *Ann Biomed Eng*. 2007; 35(4):560–581.
44. Kleinstreuer C, Zhang Z, Donohue JF. Targeted drug-aerosol delivery in human respiratory system. *Annu Rev Biomed Eng*. 2008;10:195–220.
45. Ribeiro P, Si X. Section 2: electric and magnetic circuit. In: Beaty HW, Fink DG, editors. *Standard Handbook for Electrical Engineering*. 16 ed. New York: McGraw Hill; 2012:2.1–2.58.
46. Lam K, Tan BK, Lavin JM, Meen E, Conley DB. Comparison of nasal sprays and irrigations in the delivery of topical agents to the olfactory mucosa. *Laryngoscope*. 2013;123(12):2950–2957.
47. Baquero F, Loza E. Antibiotic resistance of microorganisms involved in ear, nose and throat infections. *Pediatr Infect Dis J*. 1994;13(1): S9–S14.
48. Darquenne C. Aerosol deposition in health and disease. *J Aerosol Med Pulm Drug Deliv*. 2012;25(3):140–147.
49. Djupesland PG, Skretting A, Winderen M, Holand T. Breath actuated device improves delivery to target sites beyond the nasal valve. *Laryngoscope*. 2006;116(3):466–472.
50. Dhand R. Aerosol therapy in patients receiving noninvasive positive pressure ventilation. *J Aerosol Med Pulm Drug Deliv*. 2012;25(2):63–78.
51. Willis LD, Berlinski A. Survey of aerosol delivery techniques to spontaneously breathing tracheostomized children. *Respir Care*. 2012; 57(8):1234–1241.
52. Frey K, Unholtz D, Bauer J, et al. Automation and uncertainty analysis of a method for in-vivo range verification in particle therapy. *Phys Med Biol*. 2014;59(19):5903–5919.
53. Hyo N, Takano H, Hyo Y. Particle deposition efficiency of therapeutic aerosols in the human maxillary sinus. *Rhinology*. 1989;27(1):17–26.
54. Guo Y, Laube B, Dalby R. The effect of formulation variables and breathing patterns on the site of nasal deposition in an anatomically correct model. *Pharm Res*. 2005;22(11):1871–1878.
55. Dondeti P, Zia HS, Needham TE. In vivo evaluation of spray formulations of human insulin for nasal delivery. *Int J Pharm*. 1995;122(1–2): 91–105.
56. Teshima D, Yamauchi A, Makino K, et al. Nasal glucagon delivery using microcrystalline cellulose in healthy volunteers. *Int J Pharm*. 2002; 233(1–2):61–66.
57. Walton S, Hassan O, Morgan K, Brown MR. Modified cuckoo search: a new gradient free optimisation algorithm. *Chaos Solitons Fractals*. 2011;44(9):710–718.

International Journal of Nanomedicine

Dovepress

Publish your work in this journal

The International Journal of Nanomedicine is an international, peer-reviewed journal focusing on the application of nanotechnology in diagnostics, therapeutics, and drug delivery systems throughout the biomedical field. This journal is indexed on PubMed Central, MedLine, CAS, SciSearch®, Current Contents®/Clinical Medicine, Journal Citation Reports/Science Edition, EMBase, Scopus and the Elsevier Bibliographic databases. The manuscript management system is completely online and includes a very quick and fair peer-review system, which is all easy to use. Visit http://www.dovepress.com/testimonials.php to read real quotes from published authors.

Submit your manuscript here: http://www.dovepress.com/international-journal-of-nanomedicine-journal